# Laser-filament-induced snow formation in a subsaturated zone in a cloud chamber: Experimental and theoretical study

Jingjing Ju,[1,2] Haiyi Sun,[2] Aravindan Sridharan,[1] Tie-Jun Wang,[1,2] Cheng Wang,[2] Jiansheng Liu,[2,*] Ruxin Li,[2,†] Zhizhan Xu,[2] and See Leang Chin[1,‡]

[1]*Department of Physics, Engineering Physics and Optics and Center for Optics, Photonics and Laser (COPL), Laval University, Quebec City, QC G1V 0A6, Canada*

[2]*State Key Lab of High Laser Field Physics, Shanghai Institute of Optics and Fine Mechanics, Chinese Academy of Science, No. 390, Qinghe Road, Jiading District, Shanghai 201800, China*

(Received 19 August 2013; published 3 December 2013)

1 kHz, 2 mJ, 45 fs, 800 nm laser pulses were fired into a laboratory diffusion cloud chamber through a subsaturated zone (relative humidity ∼73%, $T \sim 4.3$ °C). After 60 min of laser irradiation, an oval-shaped snow pile was observed right below the filament center and weighed ∼12.0 mg. The air current velocity at the edge of the vortices was estimated to be ∼16.5 cm/s. Scattering scenes recorded from the side show that filament-induced turbulence were formed inside the cloud chamber with two vortices below the filament. Two-dimensional simulations of the air flow motion in two cross sections of the cloud chamber confirm that the turbulent vortices exist below the filament. Based upon this simulation, we deduce that the vortices indeed have a three-dimensional elliptical shape. Hence, we propose that inside vortices where the humidity was supersaturated or saturated the condensation nuclei, namely, $HNO_3$, $N_2^+$, $O_2^+$ and other aerosols and impurities, were activated and grew in size. Large-sized particles would eventually be spun out along the fast moving direction towards the cold plate and formed an oval-shaped snow pile at the end.

DOI: 10.1103/PhysRevE.88.062803 PACS number(s): 42.65.Jx, 42.68.Bz, 64.70.Hz

## I. INTRODUCTION

Laser filamentation in air is well known to be a dynamic balancing process between the Kerr self-focusing, self-generated plasma-induced defocusing and probably some high-order Kerr effects [1–4]. In air, this equilibrium leads to a "clamped" laser intensity [5–8] of $\sim 5 \times 10^{13}$ W/cm$^2$ inside the filament with a plasma density of $\sim 1 \times 10^{16}$/cm$^3$ [9–13]. Recently, research in atmospheric sciences involving filaments has led to interesting results with potential applications in lightning control [11,14–18], rain making [19–25], etc.

Back in 2010, the European Teramobile group fired 10 Hz, 220 mJ, 60 fs, 800 nm laser filaments in two environments to test the idea of laser-induced condensation. The first of these was a diffusion cloud chamber and the second was the outside atmosphere. Significant growth in water droplets was confirmed through measurements of particle size and density in the volume surrounding the filament [19–21]. Laser-induced water condensation was observed even the relative humidity in the surrounding environment of filaments is subsaturated (RH ∼ 70%) [21]. The condensed particle size was measured to be ∼50 $\mu$m. However, for the condensed droplets to precipitate, one needs to keep these droplets growing in size until reaching a size of ∼2 mm in diameter [26]. The great challenge is to assist further growth of the condensed droplets. This is particularly important for the laser-induced rainmaking application in a realistic atmosphere in the future. Later on in 2011, filament-induced precipitation—specifically snow and ice formation—was observed by us in Shanghai Institute of Optics and Fine Mechanics (SIOM) by firing the laser (1 kHz, 9 mJ, 50 fs, 800 nm) into the supersaturated zone (RH = 127%, $T = -29$ °C) of a laboratory diffusion cloud chamber ($50 \times 50 \times 20$ cm$^3$). About 13 mg of snow mass was obtained after 30 min of laser irradiation [22–24]. Snowflakes were measured having a typical size of ∼1.45 mm × 1.25 mm, which is in the size region of precipitation. Recently, Leisner and researchers in the European group found that, after firing 10 Hz, (170–140) mJ, (60–140) fs, 800 nm laser pulses into a cloud chamber inside which realistic conditions were simulated, filament could induce a 100 × increase of ice particle density in a few minutes [25]. This result moves laser-assisted rainmaking a step further towards its real application in air.

Sufficient evidence for laser-induced condensation and precipitation has been provided, but the underlying physical mechanisms are still not well understood. The European Teramobile group, after confirming the existence of $NO_2$ and $O_3$ gases around the filaments, proposed that the binary $H_2O$-$HNO_3$ compounds, a by-product of the laser-induced chemistry, might have been the important cloud condensation nuclei [19–21]. In another experiment investigating laser-assisted aerosol formation, $SO_2$, and $\alpha$-pinene in ppb scale were found assisting the particle formation under simulated realistic atmospheric conditions efficiently [27]. Such compounds would also exist in our cloud chamber [22–24]. Thus, these "naturally" existing atmospheric compounds and the $H_2O$-$HNO_3$ introduced by filamentation into the surrounding air would act as condensation nuclei. With more condensation nuclei included in the air, the uptake probability of water vapor onto the nuclei surfaces increased, and gradually water vapor condensed out as water droplets at the end. Under cirrus cloud conditions (−50 °C), which were stimulated in an 84.5-m$^3$ laboratory cloud chamber, laser-filament-induced

*Corresponding author: michaeljs_liu@mail.siom.ac.cn
†ruxinli@mail.shcnc.ac.cn
‡slchin@phy.ulaval.ca

 

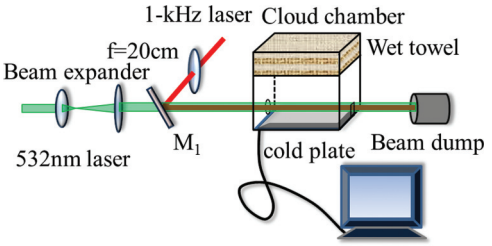


FIG. 1. (Color online) Sketch of experimental setup. $L_1$ and $L_2$ were 6 and 22.5 cm focal length lenses, respectively. $L_3$ was a 20-cm focal length lens, and $M_1$ was an 800-nm HR dichroic mirror.

ice multiplication, rather than binary $H_2O$-$HNO_3$ compounds, was proved dominate the condensation nuclei [25]. In SIOM, ion chromatography measurements of the filament-induced snow were done and results indicated the presence of $HNO_3$. This seemed to confirm the proposed interpretation of water condensation by the European group. At the same time, by adding a chopper to chop the 1 kHz pulse train into different chopping rates, the SIOM group found that higher chopping rates led to stronger laser-induced turbulence which in turn led to more and also greater precipitation in the form of snow. The strong turbulence induced by high repetition laser filaments played a crucial role in assisting the further growth in size of condensed particles, by increasing the collision probability between nuclei and water droplets [22–24].

Besides the turbulence, a supersaturated environment was also necessary to assist the further growth of condensed particles [25,28]. In this work, instead of generating filaments in a supersaturated zone, 1-kHz laser pulses were fired into a subsaturated zone (RH $\sim$ 73%, $T \sim 4.3$ °C) of a laboratory cloud chamber. Using a 20-cm focal length lens, a filament was generated at a height of 1.0 cm above the cold plate. A snow mass of $\sim$12.0 mg right below the filament was produced following 60 min of laser irradiation. Video recordings showed that the turbulence pattern below the filament contained two vortices and the maximum air current velocity on the outer edges of these vortices was estimated to be $\sim$16.5 cm/s. By assuming the laser filament as a heat source inside the cloud chamber, two-dimensional (2D) simulations of air flow motion in two cross sections were carried out. These results confirmed the existence of vortices below the filament. The possible underlying physical mechanisms of the turbulence-induced condensation and snow formation in a subsaturated zone will be discussed based upon these experimental and theoretical studies.

## II. EXPERIMENT AND RESULT

As shown in Fig. 1, laser pulses at 1 kHz, 2 mJ, 45 fs were focused into a rectangular cloud chamber ($25 \times 18 \times 15$ cm$^3$) using a biconvex lens of 20 cm focal length. A copropagating cw green laser (at 532 nm) after being expanded to a diameter of 2.0 cm by a telescope was used to probe the area around the filament. The cloud chamber walls were made of Plexiglas (transparent plastic plates). The moisture was introduced into the chamber from a compartment at the top that contained wet towels (at $\sim$19 °C) sitting on a perforated metal plate. The temperature gradient in the chamber was maintained

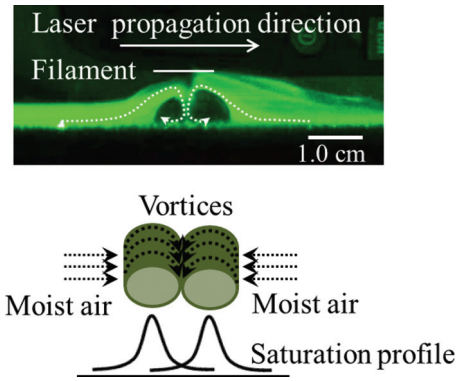


FIG. 2. (Color online) Top: Scattering scene recorded from the side with illumination of a 0.5-W green laser beam (2.0 cm in diameter) revealing two vortices below the filament. Bottom: A schematic diagram of the two vortices indicating the direction of rotation of the moist air current (top, dotted lines and curves) and the schematic radial distribution of saturation ratio inside the vortices according to [30] (bottom, solid curves).

using a cold plate (model CP-200HT-TT, TE Technology) placed at the bottom and the temperature of this plate was precisely stabilized by a computer to a value of $-19.5$ °C. Both the circular entrance window (2.0 cm diameter) and the rectangular output window (2.0 cm $\times$ 1.0 cm) were left open. The whole chamber was insulated outside with thick black foam to keep the conditions stable inside, especially the temperature gradient. The laser filament was formed at a position of 1.0 cm above the cold plate. Scattering of the probe green laser around the filament was recorded from the side from outside the chamber using a digital camera (Nikon D3200).

The zone where the laser filament was fired through was subsaturated according to the measurement taken from the hygrometer (FLUKE 971) showing a RH of $\sim$73% at a temperature ($T$) of $\sim$4.3 °C. As recorded in the Supplemental Material video [29], before firing the laser (filaments), the intensity of the side-scattered green light was very low and no particles were found around the filament position. This means that droplets with diameters $>10$ $\mu$m (the size that one pixel occupied) could not be recognized; i.e., not many particles with diameters $>10$ $\mu$m existed. After the laser was fired, a turbulence pattern with two vortices below the filament zone formed very quickly, and in a few seconds strong condensation in the form of thick clouds could be seen moving across the surface of the cold plate on both sides of the vortices.

A typical scene of the turbulence below the filament is given in Fig. 2 (top). Two vortices were found rotating next to each other in the directions indicated by the circular dotted lines in Fig. 2 (bottom). The central zones in the vortices were dark. The same method as given in [22] was used here to estimate the velocity of air current near the edges of the vortices by measuring the displacement of the scattering particles (presumably water droplets) between two subsequent frames and then multiplying with the frame rate of 25 fps. The air current velocity was found to be $\sim$16.5 cm/s. A saturation profile across the vortices is also illustrated in Fig. 2 (bottom), which is supposed to peak in the vortex cores, according to Ref. [30]. The consequence will be discussed further.

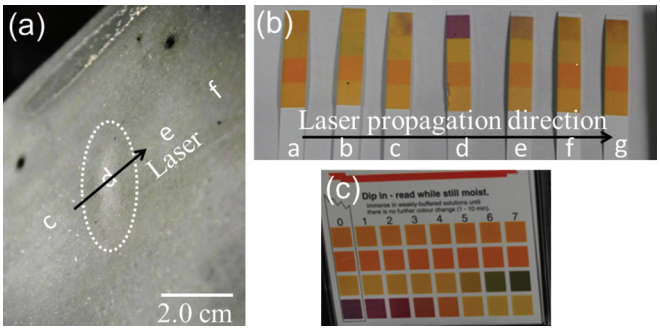


FIG. 3. (Color online) (a) Snow pile formed on the cold plate. This picture was shot with an inclined angle ∼30° relative to the cold plate. (b) Acidity of snow and ice on the cold plate measured by $p$H test papers. Positions "a"–"g" were along the laser propagation direction every 2.0 cm. Positions "a," "b," and "g" are out of the range in (a). Position "d" was where the snow pile was found. (c) Standard color card of $p$H test papers in (b). The color difference between (b) and (c) can be excluded, as they were taken at the same time.

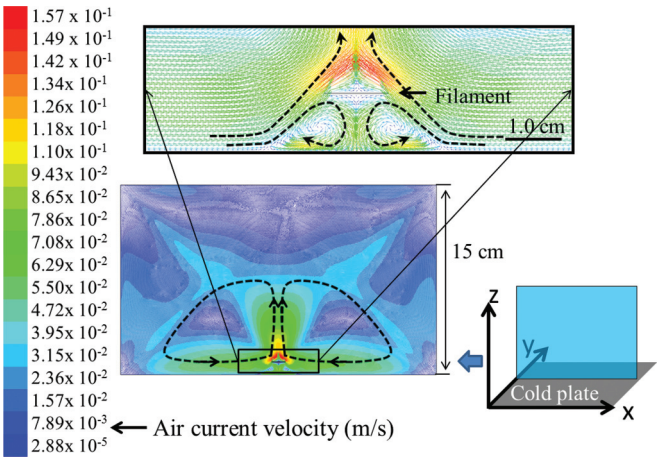


FIG. 4. (Color online) 2D simulation results of turbulence in a $x$-$z$ cross section (as indicated in the bottom right inset) containing the filament and perpendicular to the cold plate.

After the 60-min laser irradiation, a snow pile was observed right below the filament on the cold plate [Fig. 3(a)]. This pile, which took the shape of an oval, occupied an area of ∼2.0 × 0.5 cm$^2$ and weighed ∼12.0 mg. The major axis of the oval was roughly perpendicular to the filament axis. The acidity of snow and ice formation at different positions along the laser propagation on the cold plate was also measured as shown in Figs. 3(a) and 3(b). It had a maximum value of $p$H ∼ 1 at position "d" of which the laser-filament-induced snow pile occupied, i.e., right below the filament center. According to the measurements done before using ion chromatography, the main contributor to this high acidity should be the $HNO_3$ [22]. Acidity at positions "c," "e," "f," and "g" were measured around $p$H = 3–4 [Fig. 3(b)]. This is an indication that turbulence had spread the condensation seeds of $HNO_3$ (and probably other nonmeasurable seeds such as ions and dust particles) all over the cloud chamber. However, snow near the entrance window at positions "a" and "b" tested less acidic ($p$H = 6–7), which implied less $HNO_3$ had precipitated there as compared to the positions towards the exit window ("f" and "g"). This could be the consequence of the constant air flow through the opening entrance and exit window and will be further discussed later.

In nature, cloud condensation nuclei start from tiny aerosols and/or droplets of water. Heterogeneous condensation could happen under subsaturated conditions [29]. However, precipitation occurs only when the water vapor pressure exceeds the saturation vapor pressure relative to the droplet, i.e., the surrounding air should be supersaturated or saturated [29,31,32]. With no exception, snow and ice precipitation requires a saturated or supersaturated condition relative to water or ice [33]. Then one might ask how the precipitation could happen in a subsaturated zone in the present experiments. The answer seems to be effects of the turbulence together with vortex formation, which will be discussed in the next section.

## III. VORTEX-INDUCED PRECIPITATION

Simulations were done based on the assumption that the whole laser filament acts as a heat source [24,33]. The same parameters from the experiment were used in the simulation, e.g., the length of the filament was 1.10 cm and the diameter of the filament was 120 $\mu$m. As for the efficiency of the heat source, it was supposed that 5% of the laser energy in the filament was converted into heat energy [24]. The thermal decay released from the filaments has been proven to last for a few milliseconds [34], and under a 1-kHz repetition rate, laser filaments inside the cloud chamber could be treated as a constant heat source. As shown in Fig. 4 (bottom left), air flow was sucked from both the left and right sides of the filament towards its center. This was because in the filament zone, the temperature was at its peak. This caused the surrounding air to expand rapidly creating a low pressure region. One part of the sucked air went upward to form two large "loops" of air movement above the filament zone and another part of the air went downward to form two smaller loops, or vortices, as shown by the dotted lines in Fig. 4 (top right, enlarged for clarity purposes). The centers of the vortices below the filament were separated by a distance of ∼1.10 cm. These two vortices in the simulation agree well with the experimental pictures taken from the perpendicular direction (Fig. 2, top).

Our simulation results demonstrate that the heat produced by a laser filament placed in a subsaturated zone could generate an updraft towards the moist region in the top compartment of the chamber and would bring down in the return loops a flow of moist air across the whole cloud chamber. It also formed vortices below the filament (Fig. 4). In the experiment, the epicenters of these two vortices look empty (Fig. 2, top), indicating the absence of large-sized particles. The peripheral air flow circulated at a high velocity indicated by the intense scattering of large-sized traveling droplets (∼16.5 cm/s). According to Ref. [29], the high velocity of air current would help spin out large-sized particles from inside the vortices leaving behind water vapor as well as tiny water droplets whose sizes were smaller than the wavelength of the green laser (less than ∼0.5 $\mu$m) [30]. This explains why the epicenters look empty in the present experiment. Even if it was unsaturated initially, due to the decreasing demand in water vapor from the outgoing large-sized particles, the interior of the vortices would soon become saturated or even

supersaturated because of the continuous input of water vapor and tiny nanosized (hence, "invisible" in the green probe light) droplets from the turbulence (Fig. 2, bottom) [30]. With the simultaneous continual injection of cloud condensation nuclei from the filament (i.e., $HNO_3$, $N_2^+$, $O_2^+$, and impurities such as dust) via the turbulence, adsorption of water vapor on these condensation nuclei inside the vortices would occur without interruption and produce larger droplets (as long as the precipitation activation condition remained satisfied, i.e., inside the vortices it remained supersaturated or saturated). The simulation (Fig. 4, bottom left) indicates that the central updraft of air would circulate downward from the top of the chamber continually feeding the vortices with water vapor. Activated condensation nuclei would grow in size quickly. Once the particles reach a critical size, they would be spun out from the vortices and the whole process would repeat itself (saturation, supersaturation, and precipitation).

The strong condensation on both sides of the vortices, as shown in the Supplemental Material video [29], in the form of thick clouds near the cold plate could also be explained. Once the heat source, in this case the filament, was activated, thermal motion of heated air flow would produce turbulence above and below (Fig. 4). The two big "loops" of turbulence above brought the water vapor from the top compartment towards the lower region of the chamber. This in turn increased the water vapor concentration significantly in the area below the filament. Meanwhile, the temperature below the filament was relatively low (the cold plate's temperature was controlled at $-19.5\,^{\circ}$C); the "warm" water vapor from the top compartment would condense out near and above the cold surface as water droplets that took the appearance of a mist [35]. However, a current of air flew through the openings at the entrance and exit sides of the chamber. This flow of air blew the mist across the cold plate, as shown in the video, when the 1-kHz laser was blocked. This air flow will blow the $HNO_3$ generated in the filament volume to the region near the exit window. Hence, the $p$H values of snow formation near the exit window ($p$H = 3–4 at positions "f," and "g") were higher than those near the entrance window ($p$H = 6–7 at positions "a," and "b") [Fig. 3(b)].

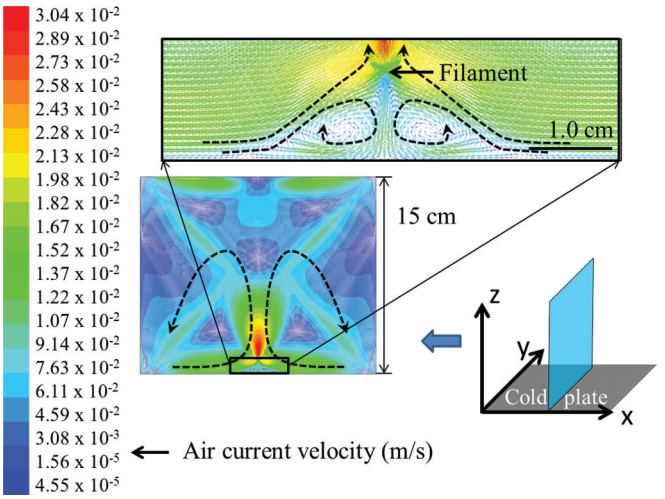


FIG. 5. (Color online) 2D simulation results of turbulence in a $y$-$z$ cross section (as indicated in the bottom right inset) cutting through the filament center and also perpendicular to the cold plate.

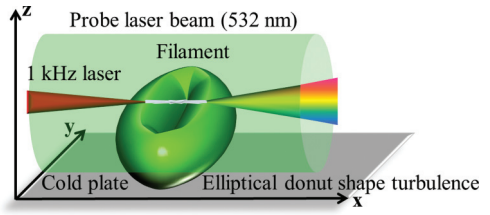


FIG. 6. (Color online) A 3D interpretation of turbulence below the filament. The $x$ axis also represents the direction of 1 kHz laser propagation, the $xy$ plane is the plane where the cold plate was, and the $z$ axis, the third dimension, is heading from the bottom to the top of the chamber.

## IV. VORTEX SHAPE

This interesting phenomenon of vortices occurring below the filament helps us understand more about the physical mechanism of condensation and precipitation when filaments are created in a subsaturated zone. Meanwhile, one could also imagine what the turbulence zone below the filament would look like based upon further simulation and experimental measurement.

In order to get a better three-dimensional picture of the whole turbulence (vortices) below the filament, another simulation was done in a cross section perpendicular to the cold plate and to the filament axis (Fig. 5). (The previous simulation was done over a section that was parallel to the filament and perpendicular to the cold plate.) From the close-up picture (Fig. 5, top right), the turbulence forms once again, below the filament, two vortices with sizes that are bigger than those in the parallel cross section (Fig. 4, top right). One can imagine now, as seen from above, the vortex below the filament would take the shape of an elliptical donut having the major axis perpendicular to the filament axis, as shown in Fig. 6.

Seen from above, this donut-shaped turbulence below the filament will look like what is illustrated on the left side of Fig. 7. Experimentally, scenes recorded from the side are shown in Fig. 7 (right) by gradually destroying the colinearity between the green laser and the filament. When the green laser was parallel to the filament, the cross sections of the

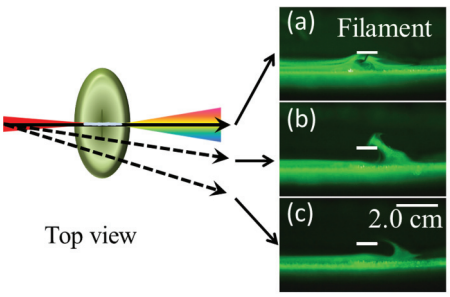


90° side scattering scenes respect to illuminating angle A, B and C.

FIG. 7. (Color online) Scenes of the donut-shaped turbulence below the filament illuminated by the green laser beam at different angles.

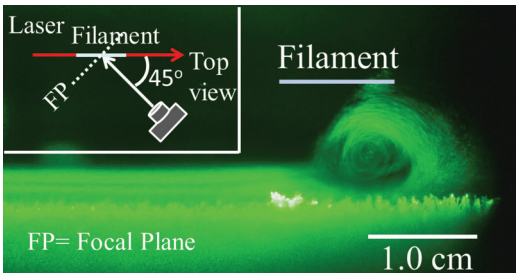


FIG. 8. (Color online) A side-scattering scene taken by the camera with a shooting angle of ∼45° with respect to the laser propagation axis, as illustrated in the inset (top left), while the probe green laser beam was collinear with the filament.

two vortices were clearly visible [Fig. 7(a)]. However, as the illumination angle was modified the cross section of the vortices became larger and elliptical as seen in the remaining two pictures [Figs. 7(b) and 7(c)]. Notwithstanding, in the experiment, the real picture of turbulence was not as perfect as the pattern predicted by the simulation. There was always a flow of air from the left to the right side inside the chamber due to the entrance and exit openings. This air motion was indicated by the motion of the mist across the surface of the cold plate as shown in the Supplemental Material video [29]. When the illumination direction was turned away from the filament axis, most of the time only a single vortex could be seen on the right-hand side, but once in a while it was possible to see both vortices appear below the filament. The vortex tube on the left side seemed to be somehow suppressed by the natural air flow.

Figure 8 presents a scattering scene taken from an angle of ∼45° with respect to the forward direction in the horizontal plane parallel to the surface of the cold plate (see the inset). While the vortex at the left side was suppressed by natural air flow as discussed before, the vortex at the right side was found moving in nice, almost circular spiral tracks, just as what was predicted in the simulation (Figs. 4 and 5). Particles (mist or condensation nuclei) carried by these vortices moved along the spiral tracks around the vortex centers. The long moving time around the spiral tracks provided them a better opportunity to collide with other particles or water molecules and grow in size. When their sizes were large enough, the large centrifugal force would spin them off the tracks and out of the vortices. According to the observation (Fig. 2, top), the air spinning speed (peripheral air flow) was high (16.5 cm/s), while in the simulation (Figs. 4 and 5), the central axial zone between the two vortex tubes was the high speed zone. It is thus highly probable that the large-sized particles were spun out principally along this axial zone towards the cold plate. This could explain why the maximum precipitation of snow was confined in an area in between the vortices and right below the filament center.

Looking at the results from the simulation, it can also be seen that the elliptical vortex tubes below the filament are longer in the direction perpendicular to the 800-nm laser (Figs. 4 and 5). This would offer a longer region with saturated or supersaturated conditions in which any cloud condensation nuclei can be activated, grow in size, and be spun out of the vortices mainly along the central axial region below the filament. This explains why the snow pile which was formed below the filament had an oval shape (2.0 cm × 0.5 cm) with the major axis perpendicular to the filament, and the minor axis dimension (0.5 cm) was smaller than the distance between the vortex centers (1.0 cm). This major axial region with fast moving air flow might also offer $HNO_3$, produced in the filament, a passageway from the filament center to the cold plate surface directly. Some of these $HNO_3$ molecules would attach on the cold plate (adsorption) without going through the next vortex motion. This would increase the acidity of the snow pile formed right below the filament center, and explains why the acidity of snow at position "d" in Fig. 3(d) was much higher than that at other positions on the cold plate.

However, the tip of the elliptical donut-shaped turbulence, which was supposed to be pointing towards the camera in a direction perpendicular to the filament, was hard to identify experimentally. The absence of this extremity of the donut-shaped turbulence in the picture can be explained by the lack of sufficiently large-sized water droplets caused by low air current velocities in that zone.

The weight of the snow formed on the whole cold plate, including the oval-shaped snow pile, was collected and weighed. The snow from the cold plate in the absence of the laser filament weighed ∼4.1 g, while it only weighed ∼3.65 g when the filament was present after 60 min of laser irradiation. Apparently, no obvious increase in the total weight of snow was found with the laser filament present when compared with the case without the laser filament for the same accumulation time. The reason was due to the constant air flow and turbulence. In the present experiment, the laser was fixed at a position of 1.0 cm from the cold plate at the bottom of the chamber. The entrance window was circular in shape with a diameter of 2.0 cm. As the laser filament was fired, the turbulence above the filament brought the moist air from the higher zones to the lower part of the cloud chamber. Water droplets mainly condensed out as mist above the cold plate within a height limited to half a centimeter, as shown in the video. Turbulence induced by the filament could cause more water droplets to move out of the chamber through the entrance and exit openings. Hence, more snow precipitation could be obtained across the whole plate when there was no filament (no turbulence).

## V. SUMMARY AND CONCLUSION

1 kHz laser pulses were focused by a 20-cm focal length lens into the subsaturated zone (RH ∼ 73%, $T$ ∼ 4.3 °C) of a laboratory diffusion cloud chamber. Laser-induced precipitation was obtained in the form of snow and its mass was measured to be ∼12.0 mg after a laser irradiation time of 60 min. From the side of the chamber with a digital camera, the turbulence pattern was recorded and two vortices could be seen below the filament. The air current velocity at the edge of the vortices was estimated to be ∼16.5 cm/s. Simulation shows the laser filament as a heat source which induced turbulence both above and below the filament. Turbulence below the filament was found, both experimentally and theoretically, to have an elliptical donut shape whose major axis was perpendicular to the laser-filament axis. The elliptical vortex tube offered a saturated or supersaturated environment inside, where the injected condensation nuclei from the filament interaction zone such as $HNO_3$, $N_2^+$, $O_2^+$, as well as other

ions and impurities could be activated. Besides that, their multiple tracks inside the vortex tubes provided the activated condensation nuclei the opportunity and time to collide with other water droplets or molecules and grow in size. Once the particles reach a critical size, they would be spun out from the vortices and with the continual feeding of moist air delivered by turbulence above the filament the whole process was able to repeat itself (saturation, supersaturation, and precipitation). The precipitation mechanism was thus sustained. This elliptical shape model of turbulence below the filament explains the observed oval shape of the snow pile very well. This work might represent an important step towards understanding the underlying physical mechanisms of laser-induced condensation and precipitation in a subsaturated region.

## ACKNOWLEDGMENTS

This work was the result of collaboration between the Center for Optics, Photonics and Laser (COPL) of Laval University and the Shanghai Institute of Optics and Fine Mechanics of the Chinese Academy of Sciences. The research work was supported in part by the following funding organizations: Natural Science and Engineering Research Council of Canada (NSERC), Canada Research Chairs, the Canada Foundation for Innovation, the Canadian Institute for Photonics Innovation, le Fonds Québécois pour la Recherche sur la Nature et les Technologies (FQRNT), the National Basic Research Program of China (Grants No. 2011CB808100 and No. 2010CB923203), National Natural Science Foundation of China (Grants No. 61221064 and No. 61008011), Shanghai science and technology talent project (12XD1405200), and the State Key Laboratory Program of Chinese Ministry of Science and Technology. One of us (S.L.C.) would like to thank T. Leisner (Institute for Meteorology and Climate Research, Karlsruhe Institute of Technology) for the advice on turbulence-induced precipitation in nature. T.J.W. also acknowledges the support from 100 Talent Program of Chinese Academy Sciences. Technical support from M. Martin of COPL is also acknowledged.

[1] S. L. Chin, *Femtosecond Laser Filamentation*, Springer Series on Atomic, Optical and Plasma Physics Vol. 55 (Springer Science Business Media, LLC, New York, 2010).
[2] S. L. Chin, S. A. Hosseini, W. Liu, Q. Luo, F. Théberge, N. Aközbek, A. Becker, V. P. Kandidov, O. G. Kosareva, and H. Schroeder, Can. J. Phys. **83**, 863 (2005).
[3] A. Couairon and A. Mysyrowicz, Phys. Rep. **441**, 47 (2007).
[4] P. Béjot, J. Kasparian, S. Henin, V. Loriot, T. Vieillard, E. Hertz, O. Faucher, B. Lavorel, and J.-P. Wolf, Phys. Rev. Lett. **104**, 103903 (2010).
[5] W. Liu, S. Petit, A. Becker, N. Aközbek, C. M. Bowden, and S. L. Chin, Opt. Commun. **202**, 189 (2002).
[6] J. Kasparian, R. Sauerbrey, and S. L. Chin, Appl. Phys. B **71**, 877 (2000).
[7] A. Becker, N. Akozbek, K. Vijayalakshmi, E. Oral, C. M. Bowden, and S. L. Chin, Appl. Phys. B **73**, 287 (2001).
[8] A. Braun, G. Korn, X. Liu, D. Du, J. Squier, and G. Mourou, Opt. Lett. **20**, 73 (1995).
[9] Y. P. Deng, J. B. Zhu, Z. G. Ji, J. S. Liu, B. Shuai, R. X. Li, Z. Z. Xu, F. Théberge, and S. L. Chin, Opt. Lett. **31**, 546 (2006).
[10] F. Théberge, W. Liu, P. T. Simard, A. Becker, and S. L. Chin, Phys. Rev. E **74**, 036406 (2006).
[11] J. Kasparian, M. Rodriguez, G. Méjean, J. Yu, E. Salmon, H. Wille, R. Bourayou, S. Frey, Y.-B. André, A. Mysyrowicz, R. Sauerbrey, J.-P. Wolf, and L. Wöste, Science **301**, 61 (2003).
[12] J. Liu, Z. Duan, Z. Zeng, X. Xie, Y. Deng, R. Li, Z. Xu, and S. L. Chin, Phys. Rev. E **72**, 026412 (2005).
[13] L. Bergé, S. Skupin, R. Nuter, J. Kasparian, and J. P. Wolf, Rep. Prog. Phys. **70**, 1633 (2007).
[14] S. L. Chin and K. Miyazaki, Jpn. J. Appl. Phys. **38**, 2011 (1999).
[15] M. Rodriguez, R. Sauerbrey, H. Wille, L. Wöste, T. Fujii, Y.-B. André, A. Mysyrowicz, L. Klingbeil, K. Rethmeier, W. Kalkner, J. Kasparian, E. Salmon, J. Yu, and J.-P. Wolf, Opt. Lett. **27**, 772 (2002).
[16] R. Ackermann, G. Méchain, G. Méjean, R. Bourayou, M. Rodriguez, K. Stelmaszczyk, J. Kasparian, J. Yu, E. Salmon, S. Tzortzakis, Y.-B. André, J.-F. Bourrillon, L. Tamin, J. P. Cascelli, C. Campo, C. Davoise, A. Mysyrowicz, R. Sauerbrey, L. Wöste, and J.-P. Wolf, Appl. Phys. B **82**, 561 (2006).
[17] R. Ackermann, K. Stelmaszczyk, P. Rohwetter, G. Méjean, E. Salmon, J. Yu, J. Kasparian, G. Méchain, V. Bergmann, S. Schaper, B. Weise, T. Kumm, K. Rethmeier, W. Kalkner, J. P. Wolf, and L. Wöste, Appl. Phys. Lett. **85**, 5781 (2004).
[18] G. Méjean, R. Ackermann, J. Kasparian, E. Salmon, J. Yu, J.-P. Wolf, K. Rethmeier, W. Kalkner, P. Rohwetter, K. Stelmaszczyk, and L. Wöste, Appl. Phys. Lett. **88**, 021101 (2006).
[19] P. Rohwetter, J. Kasparian, K. Stelmaszczyk, Z. Hao, S. Henin, N. Lascoux, W. M. Nakaema, Y. Petit, M. Queisser, R. Salam, E. Salmon, L. Wöste, and J.-P. Wolf, Nat. Photon. **4**, 451 (2010).
[20] Y. Petit, S. Henin, J. Kasparian, and J. P. Wolf, Appl. Phys. Lett. **97**, 021108 (2010).
[21] S. Hennin, Y. Petit, P. Rohwetter, K. Stelmaszczyk, Z. Q. Hao, W. M. Nakaema, A. Vogel, T. Pohl, F. Schneider, J. Kasparian, K. Weber, L. Wöste, and J. P. Wolf, Nat. Commun. **2**, 456 (2011).
[22] J. Ju, J. Liu, C. Wang, H. Sun, W. Wang, X. Ge, C. Li, S. L. Chin, R. Li, and Z. Xu, Opt. Lett. **37**, 1214 (2012).
[23] J. Ju, J. Liu, C. Wang, H. Sun, W. Wang, X. Ge, C. Li, S. L. Chin, R. Li, and Z. Xu, Appl. Phys. B **110**, 375 (2013).
[24] H. Sun, J. Liu, C. Wang, J. Ju, W. Wang, X. Ge, C. Li, S. L. Chin, R. Li, and Z. Xu, Opt. Express **21**, 9255 (2013).
[25] T. Leisner, D. Duft, O. Möhler, H. Saathoff, M. Schnaiter, S. Henin, K. Stelmaszczyk, M. Petrarca, R. Delagrange, Z. Hao, J. Lüder, Y. Petit, P. Rohwetter, J. Kasparian, J.-P. Wolf, and L. Wöste, Proc. Natl. Acad. Sci. U.S.A. **110**, 10106 (2013).
[26] N. H. Fletcher, *The Physics of Raincloud*s (Cambridge University Press, New York, 1966).
[27] H. Saathoff, S. Henin, K. Stelmaszczyk, M. Petrarca, R. Delagrange, Z. Hao, J. Lüder, O. Möhler, Y. Petit,

P. Rohwetter, M. Schnaiter, J. Kasparian, T. Leisner, J.-P. Wolf, and L. Wöste, Atmos. Chem. Phys. **13**, 4593 (2013).
[28] P. Rohwetter, J. Kasparian, L. Wöste, and J.-P. Wolf, J. Chem. Phys. **135**, 134703 (2011).
[29] See Supplemental Material at http://link.aps.org/supplemental/10.1103/PhysRevE.88.062803 for the air flow motion difference around the filament position before and after the filament fired.
[30] R. A. Shaw, J. Atmos. Sci. **57**, 3452 (2000).
[31] H. R. Pruppacher and J. D. Klett, *Microphysics of Clouds and Precipitation* (Kluwer Academic Publishers, Dordrecht, 1997).
[32] D. M. Murphy and T. Koop, Q. J. R. Meteorol. Soc. **131**, 1539 (2005).
[33] Q. Chen, Build. Environ. **31**, 233 (1995).
[34] Y.-H. Cheng, J. K. Wahlstrand, N. Jhajj, and H. M. Milchberg, Opt. Express **21**, 4740 (2013).
[35] J. L. Kate and P. Mirabel, J. Atmos. Sci. **32**, 646 (1975).